Atmos. Chem. Phys. Discuss., 15, 18653–18690, 2015
www.atmos-chem-phys-discuss.net/15/18653/2015/
doi:10.5194/acpd-15-18653-2015

Atmospheric Chemistry and Physics Discussions

Nucleation and growth of sub-3 nm particles in the polluted urban atmosphere of a megacity in China

H. Yu[1,2], L. Y. Zhou[1], L. Dai[1], W. C. Shen[1], J. Zheng[1,2], Y. Ma[1,2], and M. D. Chen[1,2]

[1]School of Environmental Science and Engineering, Nanjing University of Information Science and Technology, Nanjing, China
[2]Collaborative Innovation Center of Atmospheric Environment and Equipment Technology, Nanjing University of Information Science and Technology, Nanjing, China

Received: 22 June 2015 – Accepted: 24 June 2015 – Published: 09 July 2015

Correspondence to: H. Yu (hyu@nuist.edu.cn)

Published by Copernicus Publications on behalf of the European Geosciences Union.

Abstract

Particle size distribution down to 1.38 nm was measured in the urban atmosphere of Nanjing, China in spring, summer and winter during 2014–2015. Nucleation event occurred on 42 out of total 90 observation days, but new particles could grow to cloud condensation nuclei (CCN)-active sizes on only 9 days. In summer, infrequent nucleation was limited by both unfavorable meteorological conditions (high temperature and RH) and reduced anthropogenic precursor availability due to strict emission control measures during the 2014 Youth Olympic Games in Nanjing. The limiting factors for nucleation in winter and spring were meteorological conditions (radiation, temperature, and RH) and condensation sink, but for the further growth of sub-3 nm particles to CCN-active sizes, anthropogenic precursors again became limiting factors. Nucleation events were strong in the polluted urban atmosphere. Initial $J_{1.38}$ at the onset and peak $J_{1.38}$ at the noontime could be up to 2.1×10^2 and $2.5 \times 10^3\ \mathrm{cm^{-3}\,s^{-1}}$, respectively, during the 8 nucleation events selected from different seasons. Time-dependent $J_{1.38}$ usually showed good linear correlations with a sulfuric acid proxy for every single event (R^2 = 0.56–0.86, excluding a day with significant nocturnal nucleation), but the correlation among all the 8 events deteriorated (R^2 = 0.17) due to temperature or season change. We observed that new particle growth rate did not increase monotonically with particle size, but had a local maximum up to $25\ \mathrm{nm\,h^{-1}}$ between 1–3 nm. The growth rate behavior was interpreted in this study as the solvation effect of organic activating vapor in newly formed inorganic nuclei using nano-Köhler theory.

1 Introduction

New particle formation (NPF) is an important source of secondary aerosols in the atmosphere (Seinfeld and Pandis, 2006) and contributes significantly to the global production of cloud condensation nuclei (CCN) (Merikanto, 2009). NPF is a two-stage process consisting of homogeneous nucleation of thermodynamically stable clusters

ACPD
15, 18653–18690, 2015

and subsequent growth to detectable sizes (McMurry et al., 2005; Zhang et al., 2012). Consistent theories are still under investigation to quantify the processes physically, chemically, and dynamically (Kulmala et al., 2013, 2014). For example, the identity and physico-chemical properties of assisting vapors other than sulfuric acid (H_2SO_4) are uncertain so far. It is also uncertain what mechanisms allow the assisting vapors to overcome strong Kelvin effect over sub-3 nm particles. Existing mechanisms include condensation of extremely low volatility organic compounds (Ehn et al., 2014), nano-Köhler activation (Kulmala et al., 2004a), heterogeneous chemical reactions (Zhang and Wexler, 2002), heterogeneous nucleation (Wang et al., 2013), and adsorption of organics on cluster surface (Wang and Wexler, 2013). However, the relative importance of various mechanisms is unknown.

Direct measurements of size- and time dependent nucleation rate and growth rate in sub-3 nm size range are important to constrain the relative contributions from different mechanisms and precursors. Such measurements are also important to evaluate the survival probability of new particle to CCN-active sizes (~ 100 nm for soluble particles at 0.2 % super saturation, Pierce and Adams, 2009) and to reveal the limiting factors in the process. Recently, a series of new instruments have been developed to measure sub-3 nm aerosol number concentration and chemical composition, such as condensation particle counters (e.g., PSM, DEG-SMPS, Jiang et al., 2011a; Sipila et al., 2009; Vanhanen et al., 2011), ion spectrometers (e.g., NAIS, Asmi et al., 2009), and mass spectrometers (e.g., Cluster-CIMS, APi-TOF, CI-APi-TOF, Jokinen et al., 2012; Junninen et al., 2010; Zhao et al., 2010). Kuang et al. (2012) developed a de-coupling method to measure size- and time dependent growth rates of sub-5 nm particles. Their results at two urban sites in USA showed that size-resolved growth rates increased approximately linearly with particle size from 1 to 5 nm. Similar results were also observed in the Boreal forest (Kulmala et al., 2013; Lehtipalo et al., 2014). Based on growth rates measured below 2 nm, Kulmala et al. (2013) identified three separate size regimes, which were dominated by different key gas to particle conversion processes.

ACPD
15, 18653–18690, 2015

The relative contribution of different precursors and mechanisms to the nucleation and growth of 1–3 nm particles may vary greatly with atmospheric conditions (Riipinen et al., 2012). Therefore, sub-3 nm particle measurements in a variety of atmospheric conditions, e.g., remote or urban atmosphere, biogenic- or anthropogenic emission dominated areas, are immensely valuable. Unfortunately, such data are very sparse until now (Jiang et al., 2011b; Kuang et al., 2012; Kulmala et al., 2013; Lehtipalo et al., 2009, 2010, 2011; Yu et al., 2014a, b). China is suffering from severe atmospheric particulate matter pollution in recent years (Chan and Yao, 2008; Yue et al., 2011). To the best of our knowledge, only two studies were conducted in China to measure the occurrence of new particles down to ~ 1 nm. In these two studies, air ions (Herrmann et al., 2014) or neutral particles (Xiao et al., 2015) were measured by AIS or PSM in two urban locations of Yangtze River Delta region. Both studies were conducted in the winter season.

Here we reported the nucleation and growth of sub-3 nm particles in the urban atmosphere of Nanjing, China on arbitrarily selected observation days in spring, summer and winter of 2014–2015. Our aim was to (1) provide new insight into the initial steps of NPF based on size- and time resolved nucleation rate and growth rate measurements, and (2) shed light on possible limiting factors behind the seasonal and diurnal variations of nucleation events in the polluted urban atmosphere.

2 Methodology

2.1 Field measurements

Nanjing is the second largest megacity after Shanghai in the Yangtze River Delta (YRD) region of China (Chan and Yao, 2008). The YRD city cluster, covering 2.1×10^5 km^2 land with 170 million residents, is one of the most populated and industrialized regions in China. Field measurement was conducted from the third floor (15 m above the ground level) of an academic building beside a Chinese national meteorology ob-

ACPD
15, 18653–18690, 2015

servatory facility in NUIST campus (32.20° N, 118.71° E, (1) in Fig. 1). The sampling was carried out during the months of May (10–30 May 2014), June (01–15 June 2014), December (24–31 December 2014), February (16–22 February 2015), and March (01–07 March 2015). Total 58 measurement days were arbitrarily selected to represent spring, early summer and winter seasons, but to avoid any rain-event.

As part of an intensive summer campaign (12 August–12 September 2014), the summer measurement, using exactly the same sampling inlets, was moved to an air-conditioned trailer placed at a local governmental meteorology observatory platform (32.06° N, 118.70° E) that is 14 km south to the NUIST site ((2) in Fig. 1). The main aim of the summer campaign was to understand the effects of regional emission control measures during the 2014 Young Olympic Games (01 August–15 September) on air quality. Because the two sites locate within the same urban air shed, the measurement provided an opportunity to study seasonal variation of nucleation and its relationship with meteorological variables and gaseous precursors.

Sub-3 nm clusters/particles (hereafter referred as particles) were measured with a nano condensation nucleus counter system (nCNC) consisting of a Particle Size Magnifier (PSM model A10, Airmodus Oy, Finland) and a butanol Condensation Particle Counter (model A20, Airmodus Oy, Finland). During the measurement, an ambient air flow of 14 standard liters per minute (standard L min^{-1}) was drawn into building room or trailer via a 72 cm long and 1.0 cm I.D diameter stainless steel (SS) tube, which was extended outside the room/trailer horizontally. PSM then sampled a split flow of 2.5 standard L min^{-1} via a SS T-union. The design of the inlet tubing (length and air flow rate) was to minimize the transport loss of nano particles. The size dependent transport survival ratios of sub-3 nm particles in the inlet tubing was estimated (67–86 % for 1.38–3.0 nm) and corrected using a particle loss calculator tool (von der Weiden et al., 2009).

PSM was operated in a continuous scanning mode with a cycle of 240 steps between saturator flow rates of 0.1 and 1.0 standard L min^{-1} within 240 s. The particle cut-off sizes of the nCNC varied with saturation ratios in the saturator (Vanhanen et al.,

ACPD
15, 18653–18690, 2015

2011). A step-wise method was used to invert raw scanning data to size spectrum (time resolution: 4 min) of sub-3 nm particles, which were classified evenly into 6 size bins, i.e. 1.38–1.64, 1.64–1.90, 1.90–2.16, 2.16–2.42, 2.42–2.68, and 2.68–3.0 nm. The inverted particle number concentrations in the 6 bins were referred as $N_{1.51}$, $N_{1.77}$, $N_{2.03}$, $N_{2.29}$, $N_{2.55}$ and $N_{2.84}$, using mean values of upper and lower size boundaries in each bin. The step-wise method was described in detail by Lehtipalo et al. (2014).

Particle size distributions in the range from 3–750 nm were obtained by integrating two scanning mobility particle spectrometers (SMPS) with a nano-SMPS (a TSI differential mobility analyzer DMA3085 and a condensation particle counter CPC3776; scanning range: 3–64 nm) and a long-SMPS (TSI DMA3081 and CPC3775; scanning range: 64–750 nm). During the summer campaign, only the long-SMPS was operated to scan particles from 8–350 nm. Scanning cycles of both SMPS systems were 4 min, in order to synchronize with the nCNC. The SMPSs sampled ambient air from a separate sampling inlet. The inlet was a 129 cm long and 1.0 cm I.D horizontally-oriented SS tube with an air flow of 14 standard L min^{-1}. The transport loss of particles in the SMPS inlets was corrected using size dependent survival ratios of 85–100 % for particles > 3 nm.

Sulfur dioxide (SO_2), ozone (O_3), carbon monoxide (CO) and nitrogen oxides (NO and NO_2) concentrations were measured every 1 min with Thermo Environmental Instruments (model 43i-TLE, 49i, 48i, and 42i, respectively). When gaseous SO_2, O_3, NO_2 and CO data were not available, hourly SO_2, O_3, NO_2 and CO were obtained from nearby local Environmental Protection Agency (EPA) monitoring station. $PM_{2.5}$ was monitored with Thermo Scientific TEOM 1405. Meteorological variables including wind speed, wind direction, relative humidity (RH), temperature and solar radiation flux were recorded every 1 h during the measurement periods. Mean concentrations of $PM_{2.5}$, SO_2, and O_3 were 79 µg m^{-3}, 10 and 48 ppbv, respective, during the whole measurement period. Therefore, we regard our measurement environment as a polluted urban atmosphere.

ACPD
15, 18653–18690, 2015

2.2 Nucleation event and growth patterns

A criterion that the nCNC detected sub-3 nm particles in the atmosphere was total particle concentration reading of nCNC changed up and down periodically with scanning cut-off sizes of PSM (i.e. saturator flow rates) in scanning cycles (as shown in Fig. 2 in Lehtipalo et al., 2014). However, it was possible in the step-wise inversion method that the number concentration fluctuation of > 3 nm particles within a 4 min scanning cycle was wrongly inverted to sub-3 nm particles even when sub-3 nm particles actually did not exist according to the above criterion. As a result, the step-wise inversion method always reported a background sub-3 nm particle concentration ($N_{\text{sub-3}}$, i.e. the sum of $N_{1.51}$, $N_{1.77}$, $N_{2.03}$, $N_{2.29}$, $N_{2.55}$ and $N_{2.84}$) of 0.5×10^3–2×10^3 cm^{-3} in the nighttime and 3×10^3–8×10^3 cm^{-3} in the daytime. Similar background levels of sub-3 nm particles during non-NPF periods were also reported by other studies that used the nCNC (Kulmala et al., 2013; Lehtipalo et al., 2014; Xiao et al., 2015). Following their procedures, we did not attempt to subtract this background from $N_{\text{sub-3}}$ reported in this study.

We defined sub-3 nm particle event as sub-3 nm particle occurrence in the atmosphere for which the above criterion was fulfilled and furthermore $N_{\text{sub-3}}$ higher than background level persisted for longer than 1 h. In this study, we used sub-3 nm particle event as an approximate measure of nucleation event. This is because (1) there was an approximately positive linear correlation between $N_{\text{sub-3}}$ and nucleation rate ($J_{1.38}$ in this study, see next section) with R^2 of 0.94 (Fig. 2), and (2) $N_{\text{sub-3}}$ calculation needs only nCNC scanning data and was thus more readily available than $J_{1.38}$ calculation which needs both nCNC and SMPS scanning data. Similar definition has been discussed in our previous studies (Yu et al., 2014a, b). Apparently, a sub-3 nm particle event did not necessarily lead to an NPF event always, but it indicated the intensity and frequency of nucleation in the atmosphere. One focus in this work was to investigate the characteristics of sub-3 nm particle event.

Particle growth after nucleation is crucial to determine if nucleated particles could grow to CCN-active sizes. We identified two growth patterns according to size spec-

ACPD
15, 18653–18690, 2015

trum characteristics in sub-3 nm size range (Fig. 3). In a Type A event (Fig. 3a or b), size distribution $n(D_p, t)$ was higher at smaller sizes (e.g., 1.38–1.64 nm) than $n(D_p, t)$ at larger sizes (e.g., 2.68–3.0 nm). The size spectrum below 3 nm thus looked like a "volcano". In a Type B event (Fig. 3c or d), $n(D_p, t)$ was lower at smaller sizes than $n(D_p, t)$ at larger sizes ("up-side-down volcano"). For the size range > 3 nm, depending on whether a banana-shape growth was seen, we further defined Type A1/A2 and Type B1/B2 events: in Type A1 and B1 events, particles eventually grew to CCN-active sizes, while in Type A2 and B2 events banana-shape particle growth to CCN-active sizes was not seen. Therefore, Type A1 and B1 events were equivalent to conventional NPF events.

Type B size distribution was more unusual since $n(D_p, t)$ of small particles were less than $n(D_p, t)$ of large particles in the sub-3 nm size range. We excluded the possibility of deteriorated nCNC detection efficiencies for small particles due to high particle loading in the sample air. This is because total number concentrations of nCNC during our measurements never approached nCNC upper concentration limit 4×10^5 cm^{-3}, especially in the early stage of nucleation when total particle concentration was rather low. Our nCNC was also calibrated periodically using H_2SO_4-H_2O particles in a laboratory flow tube to ensure the detection efficiency of the nCNC.

2.3 Formation rate and growth rate calculations with a simplified GDE method

Conventional appearance time method determined growth rates (hereafter, GR) during the initial period of NPF by finding the time steps when newly-formed particles appeared at certain size bins and calculating the GR from the time differences between successive size bins (Kulmala et al., 2012; Lehtipalo et al., 2014). The appearance time method was often not applicable to the NPF event with high GR below 3 nm, due to small size intervals (e.g., 0.26 nm for our nCNC) and long time intervals (4 min time resolution in our measurement).

An example of normalized concentrations in size bins below 3 nm on 19 February 2015 was shown in Fig. 4b. First, after the onset of nucleation, particles grew out of

ACPD
15, 18653–18690, 2015

the first size bin (1.38–1.64 nm) quickly in 4 min (GR > 0.26 nm 4 min^{-1}, i.e. 3.9 nm h^{-1}) such that the maximum or 50 % of maximum $N_{1.51}$ (yellow line) appeared later than those of $N_{1.77}$ (red line) and $N_{2.03}$ (green line). This is in contrast to the case reported in the Boreal forest where particles moved into larger size bins relatively slowly with GR < 2.1 nm h^{-1} (Kulmala et al., 2013; Lehtipalo et al., 2014). Second, new particles were generated persistently from 9 a.m. to 4 p.m. (local time, UTC + 8 h) on 19 February. Maximum concentrations appeared at around 11 a.m., which was ∼ 2 h later than the onset of nucleation. Therefore, we were not able to pinpoint maximum or 50 % maximum concentrations at the onset of nucleation correctly. Similar phenomena below 3 nm were quite common in our measurements in the urban atmosphere of Nanjing, especially on cold winter days.

The rapid growth of small particles in the urban atmosphere was the motivation that we used an alternative method to calculate growth rate and formation rate. Here, we analyzed 8 events (listed in Table 1, including both Type A1/A2 and B1/B2 events) in detail, for which complete size spectra from 1.38–750 nm were available without distorted, broken or noisy data. Total 8 size bins were classified: 6 evenly-divided size bins in sub-3 nm and 2 size bins in 3–30 nm (3–10 and 10–30 nm). For an aerosol population that is growing through simultaneous condensation and coagulation, aerosol general dynamic equation (GDE) describes the evolution of number concentration in a size bin between particle diameters D_{p1} and D_{p2} ($D_{p2} > D_{p1}$) as:

$$\frac{\mathrm{d}N(D_{p1},D_{p2},t)}{\mathrm{d}t} = J\left(D_{p1},t\right) - J\left(D_{p2},t\right) - \mathrm{CoagSnk}\left(D_{p1},D_{p2},t\right) + \mathrm{CoagSrc}\left(D_{p1},D_{p2},t\right) \quad (1)$$

where $N\left(D_{p1},D_{p2},t\right)$ is the number concentration from D_{p1} to D_{p2}, inverted from nCNC or SMPS scanning data. $\mathrm{CoagSnk}\left(D_{p1},D_{p2},t\right)$ and $\mathrm{CoagSrc}\left(D_{p1},D_{p2},t\right)$ are the sink term defining the coagulation removal of particles and the source term defining the coagulation production of particles. J is condensational growth flux (i.e. particle formation rate) across the lower ($D_{p,1}$) or upper ($D_{p,2}$) boundaries of a size bin. In the first size

ACPD
15, 18653–18690, 2015

bin of 1.38–1.64 nm, $J(1.38\,\mathrm{nm}, t)$, or simply $J_{1.38}$, is the unknown formation rate of the smallest particles that we measured.

The GDE here was the same as the Eq. (1) by Kuang et al. (2012). In their method, gaseous H_2SO_4 was measured simultaneously and a constant $\mathrm{GR}(D_p, t)/\mathrm{GR}_{H_2SO_4}(D_p, t)$ ratio at a given size over time was assumed. Their $\mathrm{GR}(D_p, t)$ was then solved by fitting the GDE to the measured size distributions. In our study, however, we did not measure gaseous H_2SO_4. Instead, $J(30\,\mathrm{nm}, t)$ in the largest size bin, which is the condensational growth flux out of 30 nm, was set to zero. This simplification was valid in the four Type A2/B2 events when particles never grew to > 30 nm (04 March, 19 February, 20 and 16 May). In the rest four Type A1/B1 events (18 February, 27 December, 15 May, and 15 August), this was also valid during the early NPF period when particles did not grow out of 30 nm and during the late NPF period when particles grew out of 30 nm completely. During the middle period of events (usually around 11 a.m.–2 p.m.), $J(30\,\mathrm{nm}, t)$ was underestimated and thus $J_{1.38}$ could be regarded as a lower estimate. In the four Type A2/B2 events, our calculation showed that J_{10} was only 0–4 % of $J_{1.38}$. Xiao et al. (2015) and Kulmala et al. (2013) measured both $J_{1.5}$ and J_3 using appearance time method. Their J_3 was less than 7 % of $J_{1.5}$. Furthermore, $J_{30}/J_{1.38}$ ratio should be even smaller than $J_{10}/J_{1.38}$ or $J_3/J_{1.5}$ ratios, considering the 8 events were carefully selected to ensure all sub-30 nm particles were grown from nucleation (not emitted directly from emission sources like vehicular engine). All these evidences supported that even if J_{30} was set to 0, $J_{1.38}$ would not be underestimated more than 7 % when particles grew cross 30 nm on 18 February, 27 December, 15 May, and 15 August.

Equation (1) requires the convergence of condensational growth (J), coagulation terms (CoagSnk and CoagSrc) and the changing rate of particle number concentration ($\mathrm{d}N/\mathrm{d}t$). Using Eq. (1) we can therefore calculate the nucleation rate $J(1.38\,\mathrm{nm}, t)$ and formation rates $J(D_p, t)$ across all size bin boundaries from 1.64 to 10 nm. After the formation rates $J(D_p, t)$ were obtained, $\mathrm{GR}(D_p, t)$ was calculated from $J(D_p, t)/n(D_p, t)$, where $n(D_p, t)$ is size distribution calculated as $n(D_p, t) = \frac{\mathrm{d}N(t)}{\mathrm{d}D_p}$ for each size bin. On

ACPD
15, 18653–18690, 2015

the other hand, the appearance time method could still be applied to (1) the size range of > 3 nm where size intervals were large (2–6 nm), and (2) the size range of < 3 nm when GR was small. The results from appearance time method were also showed in the next section.

3 Results and discussion

Sections 3.1–3.4 were organized, respectively, to address the following 3 issues: (1) seasonal variation, diurnal variation and limiting factors of nucleation event (represented by sub-3 nm particle event) in the polluted urban atmosphere, (2) time- and size dependent nucleation rate and growth rate of sub-3 nm particles, and their implications for nucleation and growth mechanisms, (3) Inhibited particle growth to CCN-active sizes in strong nucleation events of Type B2.

3.1 Seasonal and diurnal variations of nucleation event

As seen from Fig. 2, there was an approximate linear correlation between $N_{\text{sub-3}}$ and $J_{1.38}$ with the slope of $N_{\text{sub-3}}/J_{1.38}$ equal to ~ 160. This seemed to suggest that the average residence time of new particles in the sub-3 nm size range was 160 s before they were scavenged due to coagulation or grew out of 3 nm. The sub-3 nm particles observed at the present work were thus formed in situ in the urban atmosphere and not likely to be carried-over by air transport. In this section we used sub-3 nm particle event as an approximate measure of nucleation.

We observed significant seasonal characteristics of nucleation event (Fig. 5). Nucleation was rare and weak in summer, while it was commonly observed in all other seasons. During our measurements from 2014 to 2015, nucleation events occurred on 81 % of all spring observation days (May 2014), 53 % in early summer (June 2014), 10 % in summer (August and September 2014), and 64 % in winter (December 2014, February and March 2015). We compared intensity ($N_{\text{sub-3}}$) and frequency of nucle-

ACPD
15, 18653–18690, 2015

ation events, as well as meteorological variables (temperature, RH, wind speed, and solar radiation flux) and gaseous pollutants (SO_2, NO_2, CO and O_3) for spring, summer and winter seasons. June was not shown in Fig. 5 for comparison, because it was a transit season from spring (May) to summer (August and September). The data were first averaged over the entire event period for each event; and we then used event-averaged data to create box and whistler plots for the 3 seasons. $PM_{2.5}$ was used here as a surrogate of condensational sink (CS), because of the more ready availability of $PM_{2.5}$ data than SMPS data.

As shown in Fig. 5, nucleation in summer was characterized by lowest frequency, lowest $N_{sub\text{-}3}$ (2.2×10^4 cm^{-3}), and short nucleation period (only 1–2 h). Strict emission control measures during the 2014 Youth Olympic Games resulted in relatively low $PM_{2.5}$ level (32 ± 8 µg m^{-3}), which should favor nucleation. However, relatively low SO_2 concentration (1.4 ± 0.6 ppbv), high temperature (26 ± 2 °C), and high RH (74.3 ± 4.2 %) might not be in favor of nucleation. A simple H_2SO_4 proxy (Radiation $\times SO_2/PM_{2.5}$) indicated that summer H_2SO_4 concentration was likely to be the lowest among the 3 seasons, which could explain low nucleation intensity/frequency.

We further examined diurnal variations of $N_{sub\text{-}3}$ and other variables on event and non-event days in winter (Fig. 6). Because nucleation in winter was characterized by Type B event ("up-side-down volcano" below 3 nm), event days were further divided to Type B1 and Type B2 events depending on whether banana-shape particle growth was seen. The difference between Type B1 and B2 was discussed later in Sect. 3.4. During the non-event days, $N_{sub\text{-}3}$ ranged from 2.4×10^3 cm^{-3} in the night to 8.0×10^3 in the day, which was close to background levels. During the event days, $N_{sub\text{-}3}$ in the night was close to that of non-event days, but could reach 8×10^4–20×10^4 cm^{-3} in the middle of the day. This was more than 10 times higher than those on the non-event days. From Fig. 6 we can see that non-event day had higher concentrations of anthropogenic precursors (indicated by SO_2, NO_2, and CO), but nucleation seemed to be limited by higher pre-existing particle surface area (indicated by $PM_{2.5}$), higher

ACPD
15, 18653–18690, 2015

temperature and RH, and lower radiation flux. Photochemistry indicators O_3 was also lower during non-event days.

Nucleation in spring was characterized by highest frequency (81 %) among all seasons. Highest gaseous pollutant concentration of (H_2SO_4 proxy, SO_2, NO_2, CO and O_3) and radiation seemed to the favorable factors to explain this. However, $N_{sub\text{-}3}$ in spring (3.3×10^4 cm^{-3}) was much lower than that in winter (11.2×10^4 cm^{-3}). Unfavorable factors included high pre-existing particle surface area ($PM_{2.5}$: 112 ± 68 µg m^{-3}) and high temperature (27 ± 4 °C) in spring. Integrating the above seasonal and diurnal variation information in Figs. 5 and 6, we tentatively identified that the limiting factors for nucleation in our urban atmosphere were (1) radiation, temperature, RH and CS in winter and spring, and (2) temperature, RH and available gaseous precursors in summer.

Out of total 90 measurement days, 04 March 2015 in winter was the only day that we observed significant nocturnal nucleation. Sunrise and sunset were at 6:29 a.m. and 6 p.m. local time on 04 March, but nucleation were observed persistently from 4 a.m.–8 p.m. $N_{sub\text{-}3}$ increased from 3.5×10^3 cm^{-3} at 4 a.m. to 6.3×10^4 cm^{-3} before sunrise. During 10–11 a.m., peak $N_{sub\text{-}3}$ reached 3×10^4 cm^{-3}, 3 times higher than the average of all other event days in winter. Apparently, nocturnal nucleation on 04 March could not be explained as carry-over of daytime particles nor being associated with photochemistry. This implied the existence of certain dark nucleation source. With our instrument capability in this work, we could not deduce any valuable information on the nocturnal nucleation mechanism, except that we found the air mass on 04 March was relatively clean (both CS and gases, mean CS: 0.15 s^{-1}), and temperature and RH (mean: 4.4 °C and 33 %) were favorable for nucleation.

3.2 Time- and size dependent nucleation rate and growth rate of sub-3 nm particles

We observed 23 Type A events and 9 Type B events during the measurements. The different size distribution patterns (Fig. 3) were probably linked to the mechanism or

ACPD
15, 18653–18690, 2015

intensity of nucleation and growth. To address this issue, we first compared the formation rates and growth rates in two types of events. Formation rates J of 1.38, 1.64, 1.9, 2.16, 2.42, 2.68 and 3 nm particles were shown in Fig. 7 (upper panels) for typical Type A and Type B events. It is obvious that $J_{1.38}$ was much higher on 18 February (Type B) than that on 15 May (Type A). A clear time dependence of J was observed. For example, $J_{1.38}$ was 60 $cm^{-3}\,s^{-1}$ at the onset of the nucleation event on 15 May and increased to 300 $cm^{-3}\,s^{-1}$ in the middle of the day. In the type B event on 19 February, the initial and peak $J_{1.38}$ were 210 and 1200 $cm^{-3}\,s^{-1}$ respectively. Therefore, our method provided more information of nucleation than conventional calculation methods that usually showed only an averaged J at the onset of a nucleation event. Our method was also different from Kulmala et al. (2013). Their time-dependent formation rate on an event day was equal to size distribution $n(D_p, t)$ times a constant growth rate at the onset of the event obtained with the appearance time method.

The diurnal variation of J implied that nucleation was probably linked to sunlight induced photochemistry. We calculated the correlations between $J_{1.38}$ and an H_2SO_4 proxy for the 8 events of our interest. The H_2SO_4 proxy was calculated following $[H_2SO_4] = 8.21 \times 10^{-3} k \times \text{Radiation} \times [SO_2]^{0.62} \times (CS \times RH)^{-0.13}$ (Eq. 8 of Mikkonen et al., 2011), where k is the temperature-dependent reaction-rate constant. Figure 8a show that good linear correlation was usually seen for every single event with R^2 ranging from 0.72 to 0.86 for 6 out of 8 events. A moderate R^2 of 0.56 was obtained for 15 August.R^2 was lowest (0.34) on 4 March 2015. This is not surprising because we know 4 March was the only day with nocturnal nucleation during the measurement period. The slopes of log $J_{1.38}$ vs. log $[H_2SO_4]$ were close to 1 in all events (0.82–1.17, excluding 4 March), indicating activation theory can explain the nucleation mechanism in our urban atmosphere.

If data points of all the 8 events were put together, the linear correlation between H_2SO_4 proxy and $J_{1.38}$ deteriorated (slope = 1.1, $R^2 = 0.17$, Fig. 8b). In spite of considerable scattering, most of data points located between $J_{1.38} = 10^{-4.1} \times [H_2SO_4]$ and $J_{1.38} = 10^{-6.3} \times [H_2SO_4]$. An interesting finding is that the scattering of $J_{1.38}$ vs. $[H_2SO_4]$

ACPD
15, 18653–18690, 2015

proxy among all 8 events was probably due to temperature or season change (Fig. 8b). More specifically, with the same level of H_2SO_4 proxy, $J_{1.38}$ was higher in winter with lower temperature than in spring/summer with higher temperature. There were two possibilities behind the deteriorated linear correlation between H_2SO_4 proxy and $J_{1.38}$: (1) inaccurate H_2SO_4 proxy and (2) other varying factors in nucleation mechanism. First, it was very likely that H_2SO_4 concentrations in our polluted urban atmosphere were overestimated by the H_2SO_4 proxy of Mikkonen et al. (2011), which was based on statistic regression of historical datasets from relatively clean Europe/USA atmosphere. The extent of overestimation may vary with the levels of predictor variables (e.g., SO_2, temperature, CS). Mean SO_2 mixing ratios were 10.5 and 7.3 ppbv in spring/summer and winter during our measurements, respectively. These were 1 order of magnitude higher than SO_2 mixing ratios at the 6 European and USA sites (mean values: 0.23–3.4 ppbv, Mikkonen et al., 2011). Our CS in the 8 events was on the order of magnitude of 10^{-2} s^{-1}, again higher than 10^{-3} s^{-1} in Mikkonen et al. (2011). Mikkonen et al. (2011) had already pointed out that the predictive ability was lower for long term data due to atmospheric condition changes in different seasons.

Second, organic condensing vapor concentrations in particle growth events were higher in winter than those in spring/summer (Table, see Sect. 3.3). If the organics were also involved in nucleation, $J_{1.38}$ should be enhanced in winter. The enhancement of nucleation by organics (most likely anthropogenic organics in our urban atmosphere) could be supported by the comparison of $J_{1.38}$ dependences on H_2SO_4 between our study and the measurements in the Boreal forest: besides possible H_2SO_4 overestimation, $J_{1.38} = 10^{-4.1} \times [H_2SO_4] - 10^{-6.3} \times [H_2SO_4]$ in our sites was much higher than $J_{1.5} = 1.06 \times 10^{-7}[H_2SO_4]^{1.1}$ in Hyytiälä during active aerosol formation periods (Kulmala et al., 2013). At last, low temperature itself might enhance nucleation in winter (Brus et al., 2011) via increasing the saturation ratios of all nucleation precursors (e.g., water, H_2SO_4, organics).

Particle size distribution $n(D_p)$ and corresponding GR (D_p) at an instant in time during the events were shown in Fig. 7 middle and lower panels. A local minimum of $n(D_p)$ at

ACPD
15, 18653–18690, 2015

2.4 nm, followed by a local maximum somewhere between 2.5 and 10 nm, was seen on 15 May 2014. Such size distribution characteristics on 15 May 2014, as well as on all other Type A event days, was also observed by Kulmala et al. (2013) in the Boreal forest (Fig. 1a and S9A in their paper) and by Jiang et al. (2011b) in the urban area of Atlanta, USA (Fig. 1 in their paper). We further examined the growth rates in the size range of 1–3 nm on 15 May 2014. It was shown that there was a local maximum of GR (D_p) at 2.4 nm. This could explain why $n(D_p)$ was increasing in 2.4–3 nm size range: when particle condensational flow out of a size bin was slowed down, it was possible that particles flowing into the size bin accumulated, leading to particle number increase in the bin.

We saw more unusual behaviors of $n(D_p)$ and GR (D_p) in the Type B event on 18 February (Fig. 7 right panels): GR (D_p) decreased monotonically in the size range of 1.38–3 nm, and accordingly $n(D_p)$ increased monotonically at the same time. A high GR (D_p) of 25 nm h^{-1} was observed at 1.64 nm and GR (D_p) decreased rapid to 1.7 nm h^{-1} at ∼ 3 nm. If we consider that GR (D_p) below 1.64 nm would eventually decrease due to strong Kelvin effect of all possible precursors (H_2SO_4 or organics), the overall trend of GR (D_p) in the Type B event was in fact the same as Type A: for the smallest clusters, growth rate was small (possibly below 1 nm h^{-1}) and increased with D_p. It reached a local maximum somewhere between 1–3 nm, after which GR (D_p) decreased with D_p. For a typical NPF event, GR (D_p) would eventually increase again after a local minimum between 3–10 nm. The difference between the Type A event (18 February) and Type B event (15 May) was the D_p of local maximum GR (D_p) (2.4 vs. 1.64 nm).

The interesting behaviors of $n(D_p)$ and GR (D_p) in our urban atmosphere were different from the stereotyped understanding that steady-state cluster size distribution $n(D_p)$ decreases with D_p in nucleation and GR increases monotonically with D_p in an NPF event. It should be pointed out that if we calculated the overall GR in 1.38–3 nm, $GR_{1.38-3}$ was 3.6 nm h^{-1} on 15 May and 4.4 nm h^{-1} on 18 February, which were still

ACPD
15, 18653–18690, 2015

smaller than GR_{3-20} during the initial period of the events (7.7 and 5.96 nm h^{-1}, calculated using appearance time method). Table 1 showed that a faster GR_{3-20} than $GR_{1.38-3}$ were quite common, except in two events on 16 and 20 May when particles did not grow beyond 3 nm. Overall, GR was still increasing with increasing D_p.

Kuang et al. (2012) had also reported a local maximum of GR at ~ 2.6 nm in an NPF event measured in Atlanta, USA (Fig. 1b in their paper). In this study we further point out that GR could decrease monotonically with D_p in 1–3 nm range in strong nucleation events. Our GR was calculated from a simplified GDE method, however, the decease of GR in 1–3 nm size range could be easily inferred from the size spectra shown in Fig. 3 or Fig. 7 (middle panels): for a D_{p2} that was larger than D_{p1}, particle formation rate $J(D_{p2})$ must be smaller than $J(D_{p1})$. If we observed a higher $n(D_{p2})$ than $n(D_{p1})$, GR (D_p) that was equal to $J(D_p)/n(D_p)$ must be smaller at D_{p2} than D_{p1}.

Apparently, the complicated growth rate behaviors in our polluted urban atmosphere can not be explained by H_2SO_4 condensation alone, not only because H_2SO_4 condensational growth rate ($GR_{H_2SO_4}$, calculated from the H_2SO_4 proxy and shown as black dashed lines in Fig. 7) was smaller than the measured growth rate ($GR_{measured}$), but also because $GR_{H_2SO_4}$ curve should follow a monotonically decreasing trend in > 1 nm sizes assuming a collision-only condensational growth without vaporization (Nieminen et al., 2010).

3.3 Growth rate due to activating vapor on newly formed nuclei in sub-3 nm sizes

Kulmala et al. (2013) has attributed the increasing $n(D_p)$ with D_p at 1.7–2.0 nm to particle activation by organic vapors using nano-Köhler theory. The theory (Anttila et al., 2004; Kulmala et al., 2004a, b) suggested that an activating organic vapor was dissolved in newly formed inorganic nulei at certain size between 1–3 nm. Equilibrium organic vapor pressure over the inorganic nuclei $C_{surface}$ was thus lowered. However, the theory was usually used to describe how the GR of 1–3 nm particles was enhanced

ACPD
15, 18653–18690, 2015

by organic vapors. Attention has never been paid to the decreasing of GR after local maximum.

Here, we continued our discussion based on the nano-Köhler theory to provide an explanation of GR behaviors observed in our urban atmosphere. The net uptake of gaseous molecules by a nanoparticle was driven by the difference of the condensational flux (governed by gas-phase concentration far from the particle C_∞) and the evaporation flux (governed by volatility). If the particle was well mixed, the volatility was directly related to C_{surface}, which was determined by the pure component saturation vapor pressure C^*, particle curvature $\exp\left(\frac{4\sigma v}{kTD_p}\right)$ and particle composition. The growth rate due to an activating organic vapor (hereafter, denoted as ELVOC, extremely low volatility organic compound) was expressed as

$$\text{GR}_{\text{ELVOC}} = \frac{\gamma}{2\rho_v}\left(1+\frac{D_v}{D_p}\right)^2\left(\frac{8kT}{\pi}\right)^{\frac{1}{2}}\left(\frac{1}{m_p}+\frac{1}{m_v}\right)^{\frac{1}{2}} m_v(C_\infty - C_{\text{surface}}) \quad (2)$$

where $C_{\text{surface}} = C^* \exp\left(\frac{4\sigma v}{kTD_p}\right)\left(x_{D_p} + \exp\left(-\varphi(D_p/D_{p0})^3\right)\right)$.

The kinetic prefactor $\frac{\gamma}{2\rho_v}\left(1+\frac{D_v}{D_p}\right)^2\left(\frac{8kT}{\pi}\right)^{\frac{1}{2}}\left(\frac{1}{m_p}+\frac{1}{m_v}\right)^{\frac{1}{2}} m_v$ was taken from Nieminen et al. (2010). x_{D_p} was the mole fraction of water-soluble ELVOC in the pseudobinary solution consisting of ELVOC and an aqueous-phase sulfate nuclei. The nuclei diameter was the D_p with local maximum GR (activation diameter, $D_{p,\,act}$). The pseudobinary solution was treated ideal in the Eq. (2). For $D_p > D_{p,\,act}$, the dilution of this pseudobinary solution made C_{surface} increase to merge with Kelvin equilibrium curve (Fig. 1 in Kulmala et al., 2004a). For $D_p < D_{p,\,act}$, the condensation of the ELVOC was in effect dominated by heterogeneous nucleation onto insoluble nuclei. Therefore, C_{surface} at D_p smaller than $D_{p,\,act}$ should also increase to merge with Kelvin equilibrium curve. To account for this effect, an empirical term $\exp\left(-\varphi(D_p/D_{p0})^3\right)$ was added to Eq. (2). Here, D_{p0} was 1 nm to cancel off the unit of D_p. If $D_p \to 0$, the term $\to 1$. If $D_p \to D_{p,\,act}$, the term $\to 0$.

ACPD
15, 18653–18690, 2015

Consequently, $C_\infty - C_{surface}$ had a local maximum at the $D_{p,\,act}$. On even larger particles > 10 nm, $C_\infty - C_{surface}$ would eventually increase due to weakened Kelvin effect. Therefore, the trend of $C_\infty - C_{surface}$ coincided with the change of GR with D_p.

We fitted GR_{ELVOC} with the measured GR in sub-3 nm sizes ($GR_{GDE\ method}$ in Fig. 9) at an instant in time by adjusting 3 free parameters in Eq. (2): C^*, C_∞, and φ. Other parameters like surface tension (0.02 N m^{-1}) and molar volume (135.5 cm^3 mol^{-1}) of ELVOC were taken from Kulmala et al. (2004a). Molecule diameter d_v (0.8 nm) and condensed-phase density ρ_v (1.5 g cm^{-3}) of ELVOC were taken from Ehn et al. (2014). Uptake coefficientγ was calculated following Nieminen et al. (2010). The fitting results in Fig. 9 showed that the dependence of $GR_{GDE\ method}$ on D_p below 3 nm could be well reproduced by Eq. (2) for both Type A and Type B events. φ ranged from 0.4–1.0 for the 8 events. Other 2 free parameters were shown in Table 1. The activating vapor concentrations C_∞ were 2.3×10^7–2.0×10^8 cm^{-3}. The saturation vapor concentration C^* were 2.5×10^6–5.7×10^7 cm^{-3}. They were within the orders of magnitude of 10^7–10^8 and 10^6–10^7 cm^{-3} suggested by Kulmala et al. (2004a), respectively.

For comparison, the GR calculated from appearance time method was also shown in Fig. 9 ($GR_{AT\ method}$) for > 3 nm particles on 15 May, 18 and 19 February, as well as for sub-3 nm particles on 20 May when particle growth was relatively slow. It can be seen that the GR on 20 May calculated from the two methods agreed well with each other, leading credit to our GDE method. $GR_{AT\ method}$ in > 10 nm sizes was usually underestimated by GR_{ELVOC}. This could be interpreted as other condensing vapors with higher volatility may contribute to particle growth in the larger particles. It should be noted that the appearance time method followed the time steps when newly-formed particles appeared in successive size bins and thus $GR_{AT\ method}$ was not the growth rates at the same instant in time.

For all the 8 nucleation events, Table 1 summarized the measured values of overall growth rate in 1.38–3 nm ($GR_{1.38-3}$), maximum growth rate in 1.38–3 nm ($GR_{max,1.38-3}$), overall growth rate in 3–20 nm (GR_{3-20}), nucleation rate ($J_{1.38}$), activation diameter ($D_{p,\,act}$), CS, and temperature (T) during the event periods with maximum nucleation

ACPD
15, 18653–18690, 2015

rates. Corresponding estimates of Mikkonen H_2SO_4 proxy, C_∞ and C^* were shown in the right 3 columns. It can be seen that in comparison with more conventional Type A events, Type B events usually occurred with (1) higher $J_{1.38}$, $GR_{max,1.38-3}$, $GR_{1.38-3}$, C_∞, and CS, (2) smaller $D_{p,\,act}$, and (3) lower T. However, the H_2SO_4 proxy and GR_{3-20} were similar in Type A and Type B events. Based on these estimations, we concluded that higher ELVOC concentration C_∞ was the key factor leading to the higher $J_{1.38}$ and $GR_{1.38-3}$, which in turn resulted in the different size spectrum pattern in Type B events ("up-side-down volcano") from in Type A events ("volcano").

It should be noted that our estimation using Eq. (2) was not a dynamic aerosol box model simulating the time evolution of growth rate. We did not consider aerosol processes explicitly, such as nucleation, coagulation and the condensation growth of H_2SO_4 and water vapors. Previous studies (e.g., Riipinen et al., 2012) suggested that water/H_2SO_4 condensation may not dominate sub-5 nm particle growth. In addition, bulk thermodynamics was applied in Eq. (2) for extremely small clusters/particles in sub-3 nm size range. All these simplifications created large uncertainties in the estimation. Therefore, our result only aimed to provide an order-of-magnitude estimation to explain the size dependence of growth rate observed in the polluted urban atmosphere.

3.4 Inhibited particle growth to CCN-active sizes in strong nucleation events of Type B2

Type B2 was strong nucleation event that produced rather high concentrations of new particles in sub-20 nm size range (Fig. 3d). High concentrations of activating vapor in these events (e.g., C_∞: 1.4–2.0 × 10^8 cm^{-3} on 18 February and 4 March) should favor a banana-shape NPF event with fast growth of particles > 20 nm, due to weakened Kelvin effect. However, it was puzzling to us why new particles accumulated in 2–20 nm and did not grow further on Type B2 event days (see Fig. 3d).

As seen from Fig. 6, meteorological variables on Type B2 days were generally more favorable in aiding particle growth than Type B1 days: lower $PM_{2.5}$, lower temperature, and higher solar radiation flux. The unfavorable factors in Type B2 events, however, in-

ACPD
15, 18653–18690, 2015

cluded lower concentrations of SO_2, NO_2, and CO (anthropogenic emission indicators), lower secondary photochemical product indicators O_3 and lower particle phase sulfate in 100–1000 nm (X. Ge, personal communication, 2015, X. Ge conducted simultaneous AMS measurement during our measurement periods). All these evidences suggested that further particle growth in Type B2 events was limited by certain condensing vapor other than ELVOC. Consequently, although there was a pool of sub-20 nm particles, they were not further "activated" due to the low availability of this condensing vapor. Following the terminology of Donahue et al. (2011, 2012), we called this condensing vapor LVOC (low volatility organic compounds)

The above hypothesis was sound if we considered that the identity of LVOC for the growth of particles > 20 nm could be different from ELVOC for sub-3 nm particle growth. Hirsikko et al. (2005) observed that GR_{3-20} demonstrated an opposite seasonal cycle to $GR_{1.3-3}$: GR_{3-20} was higher in summer, whereas $GR_{1.3-3}$ was higher in winter. This suggested that the condensing vapors were different in identity for particles of different sizes. Hirsikko et al. (2005) attributed the condensing vapors for GR_{3-20} to biogenetic VOCs. In our urban atmosphere, according to Fig. 6, LVOC was more likely to be from anthropogenic sources associated with SO_2, NO_x and CO emissions. A picture of the growth process was thus like this: ELVOC of lower volatility, lower concentration and higher water solubility activated inorganic nuclei and accelerated particle growth in smaller sizes. This in turn assisted in the condensation of LVOC of high volatility, low solubility, but with larger amount of mass. The further growth of particles > 20 nm, which means significant increment of particle mass, needed continuous supply of LVOC from the anthropogenic sources. On the Type B2 days, LVOC supply was not adequate (low SO_2, CO and NO_x). As a result, continuous banana-shape particle growth did not take place.

ACPD
15, 18653–18690, 2015

4 Conclusions

NPF can contribute to CCN only after going through nucleation, initial growth steps and subsequent growth to CCN-active sizes. This study provided the evidences of limiting factors in these processes in a polluted urban atmosphere in China. We observed atmospheric nucleation events on 42 out of total 90 observation days, but particles could grow to CCN-active sizes on only 9 days. In summer, infrequent nucleation was limited by both low concentrations of gaseous precursors and high temperature and RH. In more polluted winter and spring atmosphere, precursor supply was not limiting anymore; nucleation can occur once meteorological conditions were favorable (i.e. low CS and temperature/RH, higher solar radiation). However, for the further growth of sub-3 nm particles to CCN-active sizes, anthropogenic gaseous precursors again became limiting factors.

A simplified GDE method was used in this study to calculate particle formation rates first and then growth rates. Nucleation events were strong in the polluted urban atmosphere of Nanjing. Initial $J_{1.38}$ at the onset and peak $J_{1.38}$ at the noontime could be up to 2.1×10^{2} and 2.5×10^{3} cm^{-3} s^{-1}, respectively, during the 8 nucleation events selected from different seasons. The diurnal variation of $J_{1.38}$ implied that nucleation was usually linked to sunlight induced photochemistry. Time-dependent $J_{1.38}$ showed good linear correlations with the H_2SO_4 proxy for every single event, except a day with significant nocturnal nucleation. However, the correlation between $J_{1.38}$ and the H_2SO_4 proxy for all 8 events deteriorated, which might reflect the effect of temperature or assisting vapor concentration in the nucleation. The deteriorated correlation could also be due to the lower predictive ability of the H_2SO_4 proxy in the polluted urban atmosphere for different seasons.

In all nucleation events, a local maximum growth rate was observed between 1–3 nm with GR up to 25 nm h^{-1}. This means GR was not monotonically increasing with particle size. The overall $GR_{1.38-3}$, however, was still smaller than GR_{3-20}, if particles could grow beyond 3 nm. The local maximum growth rate was interpreted, using nano-Köhler

ACPD
15, 18653–18690, 2015

theory, as the solvation effect of organic activating vapor in newly formed inorganic nuclei. Based on our estimation, high ELVOC concentration of 2.3×10^7–2.0×10^8 cm^{-3} was expected to be the key factor leading to high $GR_{1.38-3}$. The varying GR of new particle in turn resulted in the different particle growth patterns that we observed in Nanjing.

Our results call for a more robust proxy of gaseous H_2SO_4 to be developed for polluted urban conditions. Our year-round measurement data provided valuable size evolution data of sub-3 nm clusters/particles to evaluate previous aerosol dynamic models of new particle formation. A robust dynamic model was needed to appropriately treat all aerosol and gas-phase processes in the initial growth steps.

Acknowledgements. This work was supported by National Science Foundation of China (41 405 116), Natural Science Foundation of Jiangsu Province (BK20 140 989), and Jiangsu Specially Appointed Professor grant. The measurement campaigns were partially funded by the Priority Academic Program Development of Jiangsu Higher Education Institutions (PAPD). We thank Vijay P. Kanawade and Xinlei Ge for valuable discussion.

References

Anttila, T., Kerminen, V.-M., Kulmala, M., Laaksonen, A., and O'Dowd, C. D.: Modelling the formation of organic particles in the atmosphere, Atmos. Chem. Phys., 4, 1071–1083, doi:10.5194/acp-4-1071-2004, 2004.

Asmi, E., Sipilä, M., Manninen, H. E., Vanhanen, J., Lehtipalo, K., Gagné, S., Neitola, K., Mirme, A., Mirme, S., Tamm, E., Uin, J., Komsaare, K., Attoui, M., and Kulmala, M.: Results of the first air ion spectrometer calibration and intercomparison workshop, Atmos. Chem. Phys., 9, 141–154, doi:10.5194/acp-9-141-2009, 2009.

Brus, D., Neitola, K., Hyvärinen, A.-P., Petäjä, T., Vanhanen, J., Sipilä, M., Paasonen, P., Kulmala, M., and Lihavainen, H.: Homogenous nucleation of sulfuric acid and water at close to atmospherically relevant conditions, Atmos. Chem. Phys., 11, 5277–5287, doi:10.5194/acp-11-5277-2011, 2011.

Chan, C. K. and Yao, X.: Air pollution in mega cities in China, Atmos. Environ., 42, 1–42, doi:10.1016/j.atmosenv.2007.09.003, 2008.

ACPD
15, 18653–18690, 2015

Donahue, N. M., Trump, E. R., Pierce, J. R., and Riipinen, I.: Theoretical constraints on pure vapor-pressure driven condensation of organics to ultrafine particles, Geophys. Res. Lett., 38, L16801, doi:10.1029/2011gl048115, 2011.

Donahue, N. M., Kroll, J. H., Pandis, S. N., and Robinson, A. L.: A two-dimensional volatility basis set – Part 2: Diagnostics of organic-aerosol evolution, Atmos. Chem. Phys., 12, 615–634, doi:10.5194/acp-12-615-2012, 2012.

Ehn, M., Thornton, J. A., Kleist, E., Sipila, M., Junninen, H., Pullinen, I., Springer, M., Rubach, F., Tillmann, R., Lee, B., Lopez-Hilfiker, F., Andres, S., Acir, I.-H., Rissanen, M., Jokinen, T., Schobesberger, S., Kangasluoma, J., Kontkanen, J., Nieminen, T., Kurten, T., Nielsen, L. B., Jorgensen, S., Kjaergaard, H. G., Canagaratna, M., Maso, M. D., Berndt, T., Petaja, T., Wahner, A., Kerminen, V. M., Kulmala, M., Worsnop, D. R., Wildt, J., and Mentel, T. F.: A large source of low-volatility secondary organic aerosol, Nature, 506, 476–479, doi:10.1038/nature13032, 2014.

Herrmann, E., Ding, A. J., Kerminen, V.-M., Petäjä, T., Yang, X. Q., Sun, J. N., Qi, X. M., Manninen, H., Hakala, J., Nieminen, T., Aalto, P. P., Kulmala, M., and Fu, C. B.: Aerosols and nucleation in eastern China: first insights from the new SORPES-NJU station, Atmos. Chem. Phys., 14, 2169–2183, doi:10.5194/acp-14-2169-2014, 2014.

Hirsikko, A., Laakso, L., Horrak, U., Aalto, P. P., Kerminen, V. M., and Kulmala, M.: Annual and size dependent variation of growth rates and ion concentrations in boreal forest, Boreal Environ. Res., 10, 357–469, 2005.

Jiang, J., Chen, M., Kuang, C., Attoui, M., and McMurry, P. H.: Electrical mobility spectrometer using a diethylene glycol condensation particle counter for measurement of aerosol size distributions down to 1 nm, Aerosol Sci. Tech., 45, 510–521, doi:10.1080/02786826.2010.547538, 2011a.

Jiang, J., Zhao, J., Chen, M., Eisele, F. L., Scheckman, J., Williams, B. J., Kuang, C., and McMurry, P. H.: First measurements of neutral atmospheric cluster and 1–2 nm particle number size distributions during nucleation events, Aerosol Sci. Tech., 45, II–V, doi:10.1080/02786826.2010.546817, 2011b.

Jokinen, T., Sipilä, M., Junninen, H., Ehn, M., Lönn, G., Hakala, J., Petäjä, T., Mauldin III, R. L., Kulmala, M., and Worsnop, D. R.: Atmospheric sulphuric acid and neutral cluster measurements using CI-APi-TOF, Atmos. Chem. Phys., 12, 4117–4125, doi:10.5194/acp-12-4117-2012, 2012.

ACPD
15, 18653–18690, 2015

Junninen, H., Ehn, M., Petäjä, T., Luosujärvi, L., Kotiaho, T., Kostiainen, R., Rohner, U., Gonin, M., Fuhrer, K., Kulmala, M., and Worsnop, D. R.: A high-resolution mass spectrometer to measure atmospheric ion composition, Atmos. Meas. Tech., 3, 1039–1053, doi:10.5194/amt-3-1039-2010, 2010.

Kuang, C., Chen, M., Zhao, J., Smith, J., McMurry, P. H., and Wang, J.: Size and time-resolved growth rate measurements of 1 to 5 nm freshly formed atmospheric nuclei, Atmos. Chem. Phys., 12, 3573–3589, doi:10.5194/acp-12-3573-2012, 2012.

Kulmala, M., Kerminen, V. M., Anntila, T., Laaksonen, A., and O'Dowd, C. D.: Organic aerosol formation via sulfate cluster activation, J. Geophys. Res., 109, D04205, doi:10.1029/2003JD003961, 2004a.

Kulmala, M., Laakso, L., Lehtinen, K. E. J., Riipinen, I., Dal Maso, M., Anttila, T., Kerminen, V.-M., Hõrrak, U., Vana, M., and Tammet, H.: Initial steps of aerosol growth, Atmos. Chem. Phys., 4, 2553–2560, doi:10.5194/acp-4-2553-2004, 2004b.

Kulmala, M., Petäjä, T., Nieminen, T., Sipilä, M., Manninen, H. E., Lehtipalo, K., Dal Maso, M., Aalto, P. P., Junninen, H., Paasonen, P., Riipinen, I., Lehtinen, K. E. J., Laaksonen, A., and Kerminen, V. M.: Measurement of the nucleation of atmospheric aerosol particles, Nat. Protoc., 7, 1651–1667, doi:10.1038/nprot.2012.091, 2012.

Kulmala, M., Kontkanen, J., Junninen, H., Lehtipalo, K., Manninen, H. E., Nieminen, T., Petäjä, T., Sipilä, M., Schobesberger, S., Rantala, P., Franchin, A., Jokinen, T., Järvinen, E., Äijälä, M., Kangasluoma, J., Hakala, J., Aalto, P. P., Paasonen, P., Mikkilä, J., Vanhanen, J., Aalto, J., Hakola, H., Makkonen, U., Ruuskanen, T., Mauldin, R. L., Duplissy, J., Vehkamäki, H., Bäck, J., Kortelainen, A., Riipinen, I., Kurtén, T., Johnston, M. V., Smith, J. N., Ehn, M., Mentel, T. F., Lehtinen, K. E. J., Laaksonen, A., Kerminen, V. M., and Worsnop, D. R.: Direct observations of atmospheric aerosol nucleation, Science, 339, 943–946, doi:10.1126/science.1227385, 2013.

Kulmala, M., Petäjä, T., Ehn, M., Thornton, J., Sipilä, M., Worsnop, D. R., and Kerminen, V. M.: Chemistry of atmospheric nucleation: on the recent advances on precursor characterization and atmospheric cluster composition in connection with atmospheric new particle formation, Annu. Rev. Phys. Chem., 65, 21–37, doi:10.1146/annurev-physchem-040412-110014, 2014.

Lehtipalo, K., Sipilä, M., Riipinen, I., Nieminen, T., and Kulmala, M.: Analysis of atmospheric neutral and charged molecular clusters in boreal forest using pulse-height CPC, Atmos. Chem. Phys., 9, 4177–4184, doi:10.5194/acp-9-4177-2009, 2009.

ACPD
15, 18653–18690, 2015

Lehtipalo, K., Kulmala, M., Sipilä, M., Petäjä, T., Vana, M., Ceburnis, D., Dupuy, R., and O'Dowd, C.: Nanoparticles in boreal forest and coastal environment: a comparison of observations and implications of the nucleation mechanism, Atmos. Chem. Phys., 10, 7009–7016, doi:10.5194/acp-10-7009-2010, 2010.

Lehtipalo, K., Sipila, M., Junninen, H., Ehn, M., Berndt, T., Kajos, M. K., Worsnop, D. R., Petaja, T., and Kulmala, M.: Observations of nano-CN in the nocturnal boreal forest, Aerosol Sci. Tech., 45, 499–509, doi:10.1080/02786826.2010.547537, 2011.

Lehtipalo, K., Leppä, J., Kontkanen, J., Kangasluoma, J., Franchin, A., Wimmer, D., Schobesberger, S., Junninen, H., Petäjä, T., Sipilä, M., Mikkilä, J., Vanhanen, J., Worsnop, D. R., and Kulmala, M.: Methods for determining particle size distribution and growth rates between 1 and 3 nm using the Particle Size Magnifier, Boreal Environ. Res., 19, 215–236, 2014.

McMurry, P. H., Fink, M., Sakuri, H., Stolzenburg, M., Mauldin III, R. L., Smith, J., Eisele, F. L., Moore, K., Sjostedt, S., Tanner, D., Huey, L. G., Nowak, J. B., Edgerton, E., and Voisin, D.: A criterion for new partricle formation in the sulfur-rich Atlanta atmosphere, J. Geophys. Res., 110, D22S02, doi:10.1029/2005JD005901, 2005.

Merikanto, J., Spracklen, D. V., Mann, G. W., Pickering, S. J., and Carslaw, K. S.: Impact of nucleation on global CCN, Atmos. Chem. Phys., 9, 8601–8616, doi:10.5194/acp-9-8601-2009, 2009.

Mikkonen, S., Romakkaniemi, S., Smith, J. N., Korhonen, H., Petäjä, T., Plass-Duelmer, C., Boy, M., McMurry, P. H., Lehtinen, K. E. J., Joutsensaari, J., Hamed, A., Mauldin III, R. L., Birmili, W., Spindler, G., Arnold, F., Kulmala, M., and Laaksonen, A.: A statistical proxy for sulphuric acid concentration, Atmos. Chem. Phys., 11, 11319–11334, doi:10.5194/acp-11-11319-2011, 2011.

Nieminen, T., Lehtinen, K. E. J., and Kulmala, M.: Sub-10 nm particle growth by vapor condensation – effects of vapor molecule size and particle thermal speed, Atmos. Chem. Phys., 10, 9773–9779, doi:10.5194/acp-10-9773-2010, 2010.

Pierce, J. R. and Adams, P. J.: Uncertainty in global CCN concentrations from uncertain aerosol nucleation and primary emission rates, Atmos. Chem. Phys., 9, 1339–1356, doi:10.5194/acp-9-1339-2009, 2009.

Riipinen, I., Yli-Juuti, T., Pierce, J. R., Petaja, T., Worsnop, D. R., Kulmala, M., and Donahue, N. M.: The contribution of organics to atmospheric nanoparticle growth, Nature Geosci., 5, 453–458, doi:10.1038/NGEO1499, 2012.

ACPD
15, 18653–18690, 2015

Seinfeld, J. H. and Pandis, S. N.: Atmospheric Chemistry and Physics: From Air Pollution to Climate Change, 2nd Edn., John Wiley and Sons. Inc., New York, 2006.

Sipila, M., Lehtipalo, K., Attoui, M., Neitola, K., Petäjä, T., Aalto, P. P., O'Dowd, C. D., and Kulmala, M.: Laboratory verification of PH-CPC's ability to monitor atmospheric sub-3 nm clusters, Aerosol Sci. Tech., 43, 126–135, doi:10.1080/02786820802506227, 2009.

Vanhanen, J., Mikkila, J., Lehtipalo, K., Sipila, M., Manninen, H. E., Siivola, E., Petaja, T., and Kulmala, M.: Particle size magnifier for nano-CN detection, Aerosol Sci. Tech., 45, 533–542, doi:10.1080/02786826.2010.547889, 2011.

von der Weiden, S.-L., Drewnick, F., and Borrmann, S.: Particle Loss Calculator – a new software tool for the assessment of the performance of aerosol inlet systems, Atmos. Meas. Tech., 2, 479–494, doi:10.5194/amt-2-479-2009, 2009.

Wang, J. and Wexler, A. S.: Adsorption of organic molecules may explain growth of newly nucleated clusters and new particle formation, Geophys. Res. Lett., 11, 2834–2838, doi:10.1002/grl.50455, 2013.

Wang, J., McGraw, R. L., and Kuang, C.: Growth of atmospheric nano-particles by heterogeneous nucleation of organic vapor, Atmos. Chem. Phys., 13, 6523–6531, doi:10.5194/acp-13-6523-2013, 2013.

Xiao, S., Wang, M. Y., Yao, L., Kulmala, M., Zhou, B., Yang, X., Chen, J. M., Wang, D. F., Fu, Q. Y., Worsnop, D. R., and Wang, L.: Strong atmospheric new particle formation in winter in urban Shanghai, China, Atmos. Chem. Phys., 15, 1769–1781, 2015, http://www.atmos-chem-phys.net/15/1769/2015/.

Yu, H., Gannet Hallar, A., You, Y., Sedlacek, A., Springston, S., Kanawade, V. P., Lee, Y. N., Wang, J., Kuang, C., McGraw, R. L., McCubbin, I., Mikkila, J., and Lee, S. H.: Sub-3 nm particles observed at the coastal and continental sites in the United States, J. Geophys. Res.-Atmos., 119, 2013JD020841, doi:10.1002/2013jd020841, 2014a.

Yu, H., Ortega, J., Smith, J. N., Guenther, A. B., Kanawade, V. P., You, Y., Liu, Y., Hosman, K., Karl, T., Seco, R., Geron, C., Pallardy, S. G., Gu, L., Mikkilä, J., and Lee, S. H.: New particle formation and growth in an isoprene-dominated ozark forest: from sub-5 nm to CCN-active sizes, Aerosol Sci. Tech., 48, 1285–1298, doi:10.1080/02786826.2014.984801, 2014b.

Yue, D. L., Hu, M., Zhang, R. Y., Wu, Z. J., Su, H., Wang, Z. B., Peng, J. F., He, L. Y., Huang, X. F., Gong, Y. G., and Wiedensohler, A.: Potential contribution of new particle formation to cloud condensation nuclei in Beijing, Atmos. Environ., 45, 6070–6077, doi:10.1016/j.atmosenv.2011.07.037, 2011.

ACPD
15, 18653–18690, 2015

Zhang, K. M. and Wexler, A. S.: A hypothesis for growth of fresh atmospheric nuclei, J. Geophys. Res., 107, 4577, doi:10.1029/2002JD002180, 2002.
Zhang, R., Khalizov, A., Wang, L., Hu, M., and Xu, W.: Nucleation and growth of nanoparticles in the atmosphere, Chem. Rev., 112, 1957–2011, doi:10.1021/cr2001756, 2012.
Zhao, J., Eisele, F. L., Titcombe, M., Kuang, C., and McMurry, P. H.: Chemical ionization mass spectrometric measurements of atmospheric neutral clusters using the cluster-CIMS, J. Geophys. Res., 115, D08205, doi:10.1029/2009JD012606, 2010.

ACPD
15, 18653–18690, 2015

Table 1. Activation diameter ($D_{p,\,act}$), maximum growth rate in 1.38–3 nm ($GR_{max,1.38-3}$), overall growth rate in 1.38–3 nm ($GR_{1.38-3}$), overall growth rate in 3–20 nm (GR_{3-20}), nucleation rate ($J_{1.38}$), condensation sink (CS), and temperature (T) of selected nucleation events. Estimated gas-phase activating vapor concentrations C_∞, pure saturation concentration of activating vapor over flat surface C^*, and Mikkonen H_2SO_4 proxy were shown in right 3 columns. All data were for the time periods with maximum nucleation rates.

Type	Date	$D_{p,\,act}$ (nm)	$GR_{max,1.38-3}$ ($nm\,h^{-1}$)	$GR_{1.38-3}$ ($nm\,h^{-1}$)	GR_{3-20} ($nm\,h^{-1}$)	$J_{1.38}$ ($cm^{-3}\,s^{-1}$)	T (°C)	CS (s^{-1})	Mikkonen H_2SO_4 proxy (cm^{-3})	C_∞ (cm^{-3})	C^* (cm^{-3})
A1	15 May 2014	2.42	6.4	3.6	7.7	299	20.8	1.60	8.7×10^7	5.1×10^7	6.3×10^6
A1	15 Aug 2014	2.42	14.5	7.1	7.7	201	26.1	1.81	9.3×10^7	1.1×10^8	2.5×10^7
A2	16 May 2014	2.42	3.8	1.9	0	95	25.3	1.88	1.4×10^8	3.0×10^7	4.0×10^6
A2	20 May 2014	2.16	2.9	1.6	0	92	24.1	1.87	3.8×10^7	2.3×10^7	2.5×10^6
B1	18 Feb 2015	1.64	25.9	4.4	6.0	1155	8.2	3.33	3.9×10^7	1.7×10^8	3.5×10^7
B1	27 Dec 2014	1.64	17.7	4.2	5.5	188	7.6	2.85	3.5×10^7	1.2×10^8	2.8×10^7
B2	19 Feb 2015	1.90	25.0	8.9	10.1	800	7.4	3.23	3.7×10^7	2.0×10^8	5.7×10^7
B2	04 Mar 2015	1.90	18.0	5.8	8.7	2506	3.9	2.18	4.8×10^7	1.4×10^8	2.0×10^7

ACPD
15, 18653–18690, 2015

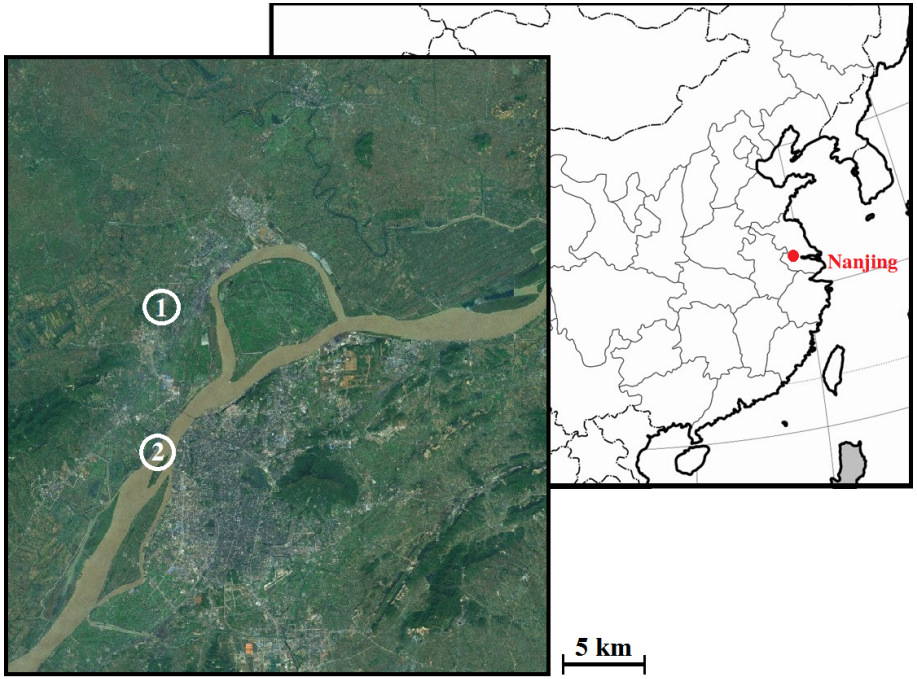

Figure 1. Locations of two urban measurement sites in Nanjing, the second largest megacity in the Yangtze River Delta region, China. (1) is the NUIST site and (2) is the summer measurement site.

ACPD
15, 18653–18690, 2015

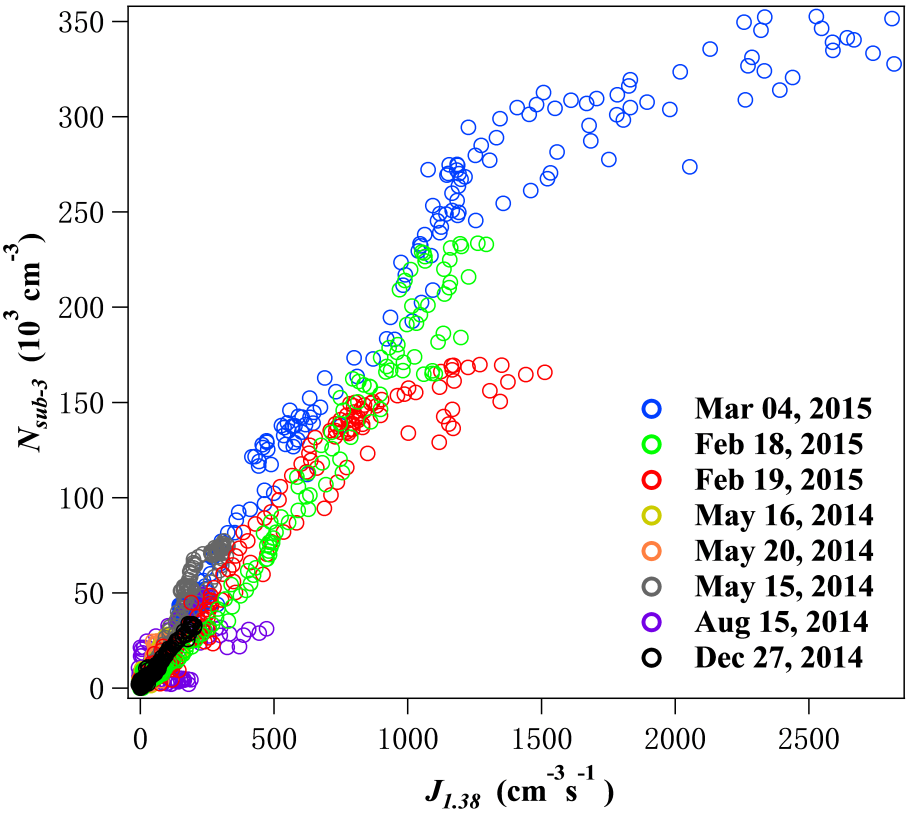

Figure 2. $N_{\text{sub-3}}$ vs. $J_{1.38}$ in the 8 nucleation events in February, May, December and August during 2014–2015. The events were indicated by different colors (blue: 01 March 2015; green: 18 February 2015; red: 19 February 2015; purple: 15 August 2014; black: 27 December 2014; grey: 15 May 2014; orange: 20 May 2014; yellow: 16 May 2014).

ACPD
15, 18653–18690, 2015

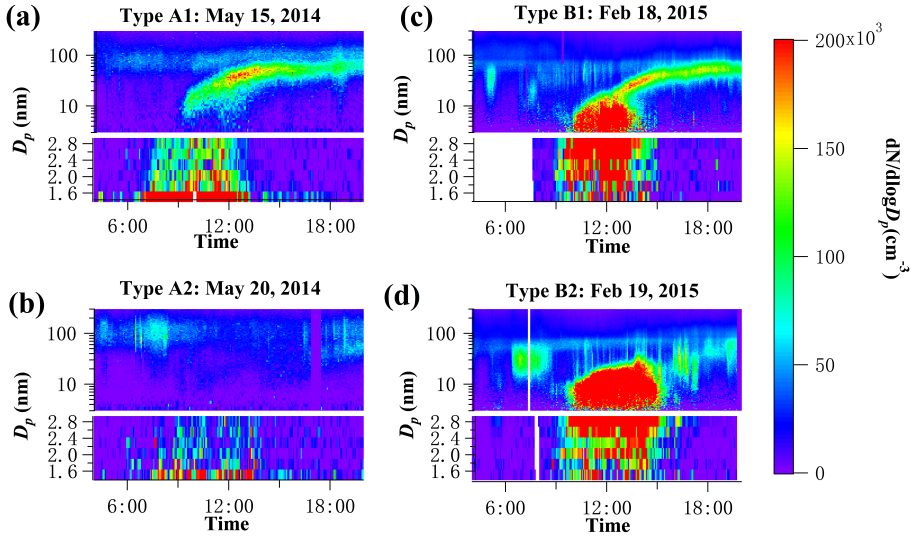

Figure 3. Size spectra of typical **(a)** Type A1 event on 15 May 2014; **(b)** Type A2 event on 20 May 2014; **(c)** Type B1 event on 18 February 2015 and **(d)** Type B2 event on 19 February 2015 during our measurement period. Size spectra from 3–300 nm (logarithmic scale) and 1.38–3 nm (linear scale) were obtained using SMPS and nCNC, respectively.

ACPD
15, 18653–18690, 2015

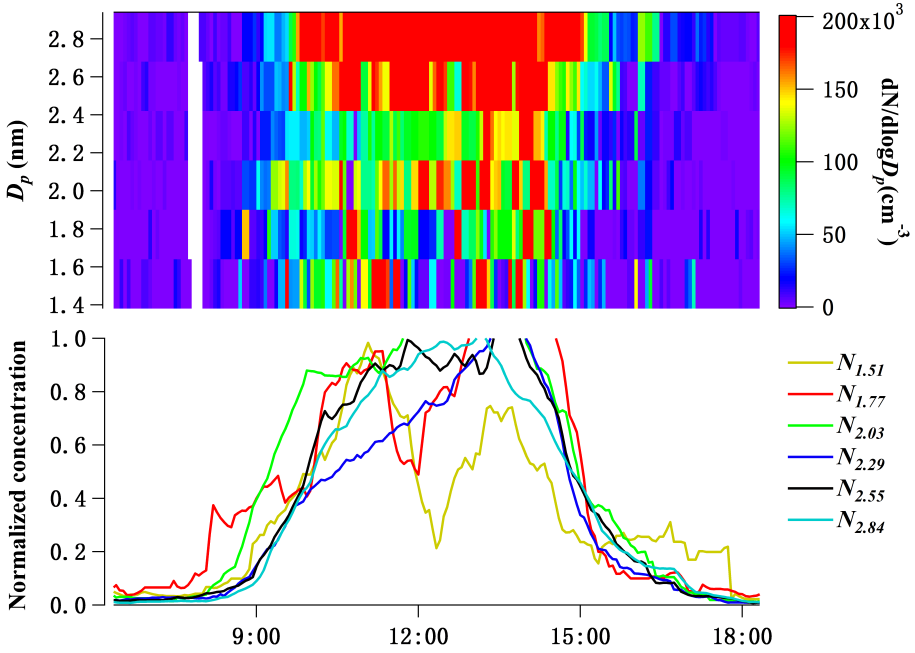

Figure 4. Upper: an example of size spectrum below 3 nm when particle growth was fast on 19 February 2015. Lower: normalized concentration in each size bin on the same day.

ACPD
15, 18653–18690, 2015

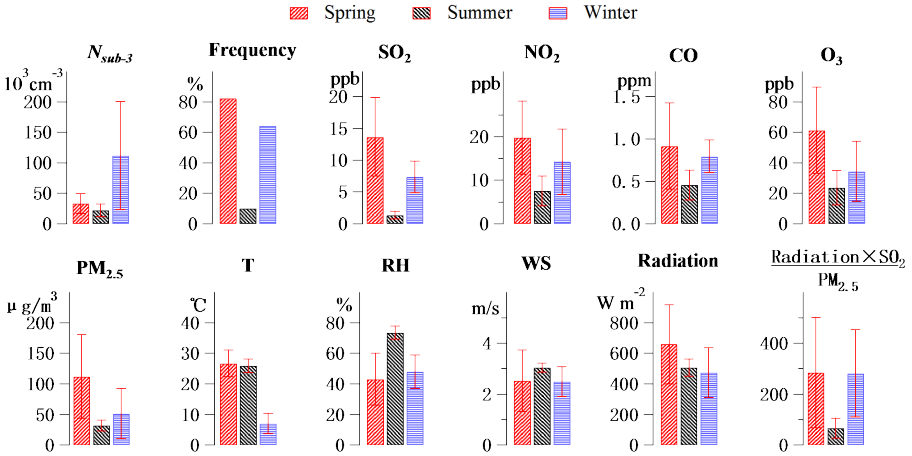

Figure 5. Mean and standard deviation of event-averaged $N_{\text{sub-3}}$, anthropogenic trace gases (SO_2, NO_2, CO and O_3), $PM_{2.5}$, and meteorological variables (temperature, RH, wind speed (WS), solar radiation, and radiation $\times SO_2/PM_{2.5}$) for nucleation events in spring (n = 17), summer (n = 3) and winter (n = 14). Nucleation frequency (the percentage of event days out of total measurement days) was also shown.

ACPD
15, 18653–18690, 2015

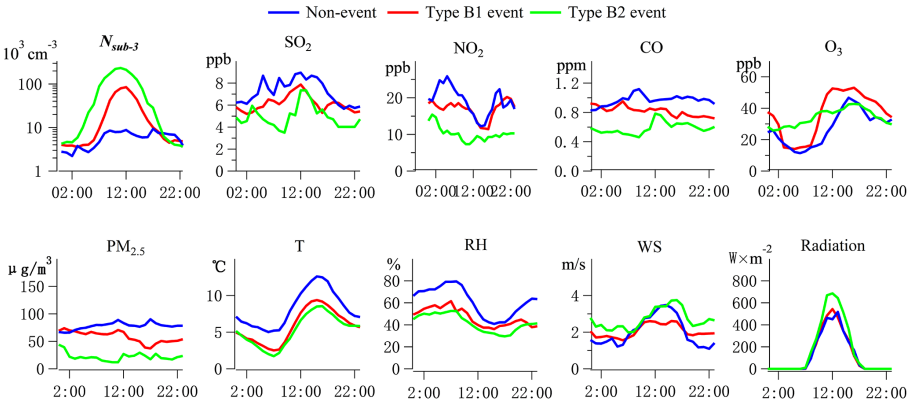

Figure 6. Diurnal variations of mean N_{sub-3}, anthropogenic trace gases (SO_2, NO_2, CO and O_3), $PM_{2.5}$, and meteorological variables (temperature, RH, wind speed, and solar radiation flux) on non-event days (n = 8, blue line) and event days (n = 3 for Type B1 event, red line and n = 6 for Type B2 event, green line) during winter measurement period.

ACPD
15, 18653–18690, 2015

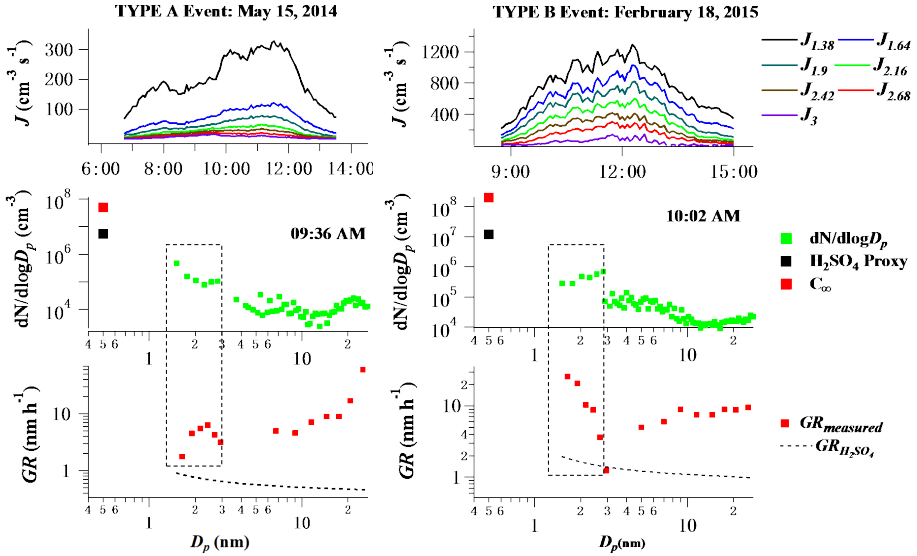

Figure 7. Upper: formation rates (or equivalently, particle growth fluxes) of 1.38, 1.64, 1.9, 2.16, 2.42, 2.68 and 3 nm cluster/particles on 15 May 2014 (Type A1 event) and 18 February 2015 (Type B1 event). Middle: particle size distribution ($dN/d\log D_p$, green square) selected during the two events (9:36 a.m. and 10:02 a.m.). Lower: particle growth rates measured during the same time periods ($GR_{measured}$, red square). Also shown in the figure were H_2SO_4 proxy (black square) and growth rates calculated from the H_2SO_4 proxy ($GR_{H_2SO_4}$, dashed black line), as well as the calculated ELVOC concentration (C_∞, red square) during the same time periods. Dashed boxes in the lower panels highlighted the size distributions and growth rates between 1.38 and 3 nm measured with nCNC.

ACPD
15, 18653–18690, 2015

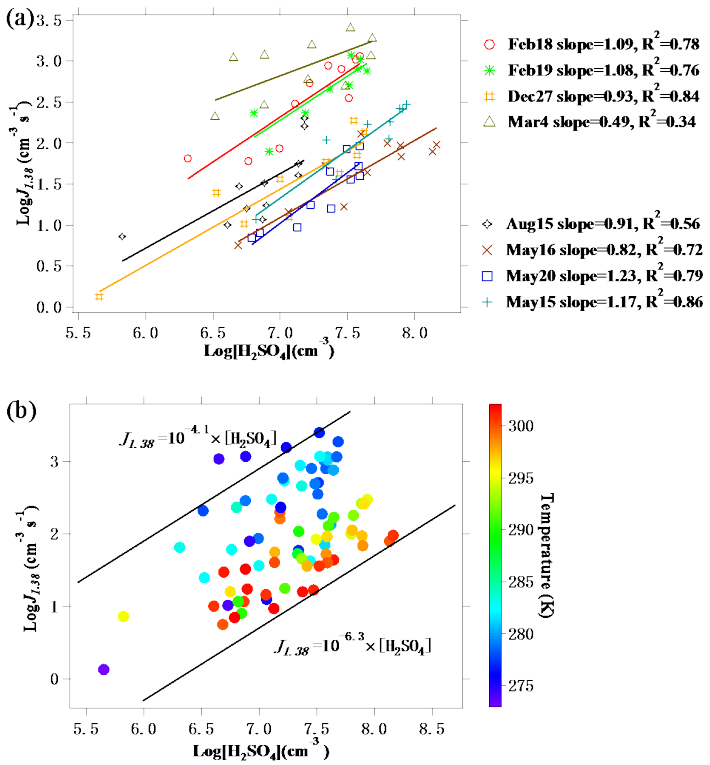

Figure 8. (a) Correlations between log $J_{1.38}$ and log [H_2SO_4] for the 8 events. H_2SO_4 proxy was calculated according to Mikkonen et al. (2011). $J_{1.38}$ and [H_2SO_4] were synchronized to 1 h that was the time resolution of solar radiation data. The colored lines showed linear fits to the data of every single event. **(b)** The same dataset as **(a)**, but with symbol color to indicate ambient temperature. Two black lines showed the linear dependences of $J_{1.38} = 10^{-4.1} \times [H_2SO_4]$ and $J_{1.38} = 10^{-6.3} \times [H_2SO_4]$, between which most of data points located.

ACPD
15, 18653–18690, 2015

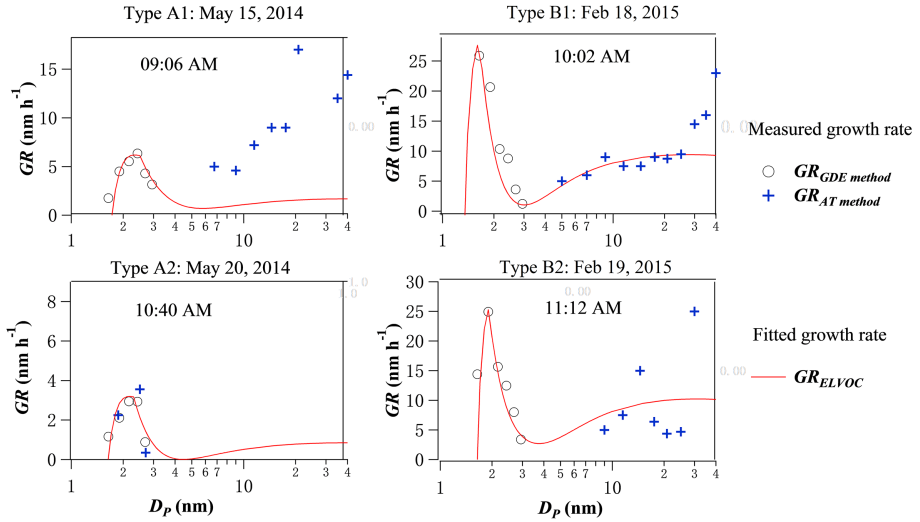

Figure 9. Comparisons of measured ($GR_{GDE\ method}$, black circle) and fitted (GR_{ELVOC}, red line) growth rates from Eq. (2) for typical Type A1, A2, B1, and B2 events. Also shown were growth rates calculated from appearance time method ($GR_{AT\ method}$, blue cross) for sub-3 nm particles when growth rate was relatively small or for larger particles with large size intervals.

ACPD
15, 18653–18690, 2015